

Modern Physics Letters A  
 © World Scientific Publishing Company

## Nuclear structure study with core excitations in Ni region: for $fp_{g9/2}$ space

P.C. SRIVASTAVA\*

*Department of Physics, University of Allahabad, Allahabad-211002, India,*

*Grand Accélérateur National d'Ions Lourds (GANIL), CEA/DSM-CNRS/IN2P3, BP 55027,  
 F-14076 Caen Cedex 5, France, and*

*Instituto de Ciencias Nucleares, Universidad Nacional Autónoma de México, 04510 México,  
 D.F., México*

Shell model calculations for Ni, Cu and Zn isotopes by modifying  $fp_g$  interaction due to Sorlin *et al.*, [Phys. Rev. Lett. 88, 092501 (2002)] have been reported. In the present work 28 two body matrix elements of the earlier interaction have been modified. Present interaction is able to explain new experimental results for this region.

*Keywords:* Large scale; Collectivity.

PACS 21.60.Cs; 27.50.+e

### 1. Introduction

The nickel isotopes ( $Z = 28$ ) cover three doubly-closed shells with number  $N = 28$ ,  $N = 40$ ,  $N = 50$  and therefore a unique testing ground to investigate the evolution of shell structure. The  $^{68}\text{Ni}$  and its neighboring attracted the interest of recent research to answer the magicity versus superfluidity question related to doubly magic character of this nuclei. <sup>1,2,3,4,5</sup> For the copper isotopes, the important question is related to rapid reduction in the energy of  $5/2^-$  state as the filling of neutrons started in the  $\nu g_{9/2}$  orbital. <sup>6,7,8,9,10,11</sup> In the Cu isotopes as  $N \sim 40$ , the state reveal three types of structures – single-particle, collective or coupling of single proton with neighboring even Ni isotopes. In the Zn isotopes with two protons more than the semi-magic  $Z = 28$  nickel nuclei, the spherical  $N = 40$  gap may not be strong enough to stabilize the nuclei in spherical shape when protons are added to the  $^{68}\text{Ni}$  core. Thus  $B(E2)$  value is larger in the chain of Zn isotopes. To understand the evolution of nuclear structure, the importance of monopole term from the tensor force is pointed out by Otsuka *et al.* <sup>12,13</sup>

The experimental  $E(2_1^+)$  for  $Z = 28$  to  $Z = 36$  are shown in Fig. 1. In this figure  $E(2_1^+)$  states in Zn are overall lower compared to Ni and an additional decrease of

\*praveen.srivastava@nucleares.unam.mx

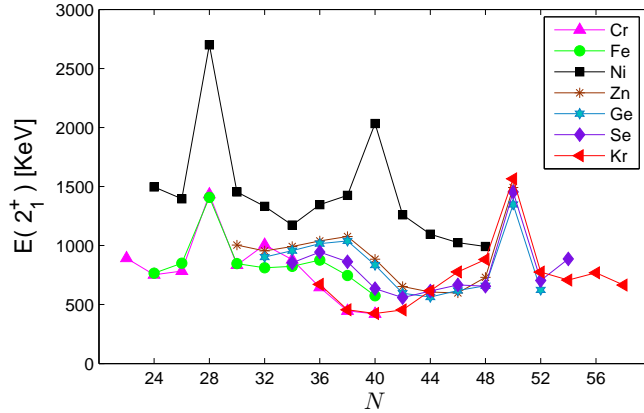
2 *P.C. Srivastava*

Fig. 1. Systematic of the experimentally observed  $E(2_1^+)$  for  $Z = 28$  to  $Z = 36$  near the  $N = 28, 40$  and  $50$  shell closure.

the  $E(2_1^+)$  energy in Zn isotopes is obtained between  $N=40-50$  compared to  $N=28-40$ . This figure also reveal the enhancement of collectivity beyond  $Z = 30$ , because of rapid decrease of  $E(2^+)$ . Below the Ni chain, the spectroscopy of Cr, Fe isotopes shown an increased collectivity toward  $N = 40$ , revealing the collapse of this shell closure. <sup>14,15</sup>

Following our recent shell-model (SM) studies for neutron-rich F isotopes <sup>16</sup>, odd and even isotopes of Fe <sup>17,18</sup>, odd-odd Mn isotopes <sup>19</sup>, odd-mass <sup>61,63,65</sup>Co isotopes <sup>20</sup>, and odd-even <sup>71-81</sup>Ga isotopes <sup>21</sup>, in the present work, large scale shell model calculations have been performed for neutron rich Ni, Cu and Zn isotopes for  $40 \leq N \leq 50$  in  $fp_{g_{9/2}}$  model space. The low-lying energy levels and  $B(E2)$  values have been calculated and compared with the recent experimental data.

The paper is organized as follows: In Section 2 details of calculation are described. In Section 3 results and discussion are presented. Finally in Section 4 we give conclusions.

## 2. Details of Calculation

Large scale shell model calculations have been performed for neutron rich nickel, copper and zinc isotopes with  $40 \leq N \leq 50$  using <sup>40</sup>Ca as a core by including the  $f_{7/2}$  orbit. In the previous work <sup>22</sup>, large scale shell model calculations were performed for neutron rich nickel, copper and zinc isotopes for  $40 \leq N \leq 50$ , using three different versions <sup>23,24,25,26,27</sup> of effective interactions for the model space consisting of the  $p_{3/2}$ ,  $p_{1/2}$ ,  $f_{5/2}$  and  $g_{9/2}$ . Both, however, yield unsatisfactory results in certain aspects, viz.

- (i) large  $E(2^+)$  value for very neutron rich nuclei (<sup>76</sup>Ni and <sup>80</sup>Zn),
- (ii) small  $B(E2)$  values in comparison to experimental values, and

(iii) for  $^{75}\text{Cu}$ ,  $^{77}\text{Cu}$  and  $^{79}\text{Cu}$ , the ground state is  $3/2^-$  as compared to the experimental indication of  $5/2^-$ .

This is probably due to neglect of the  $f_{7/2}$  orbit for the protons. In view of this,  $f_{7/2}$  orbit has been included in the valence space of protons by taking  $^{40}\text{Ca}$  as core. Effective interaction for  $fp$  valence space for both protons and neutrons with  $^{40}\text{Ca}$  as core has been constructed by Sorlin *et al.*<sup>2</sup> The main drawback of this interaction is that the effective proton single-particle energies of  $f_{7/2}$  orbital become lower than  $f_{5/2}$  which is not realistic. In the present work, we have modified relevant matrix elements to account for this discrepancy.

### 2.1. Model space

In the present work, we have used  $fp$  model space comprising of the  $0f_{7/2}$ ,  $1p_{3/2}$ ,  $0f_{5/2}$ ,  $1p_{1/2}$  active proton orbitals and  $0f_{7/2}$ ,  $1p_{3/2}$ ,  $0f_{5/2}$ ,  $1p_{1/2}$ ,  $0g_{9/2}$  neutron orbitals with eight  $f_{7/2}$  frozen neutrons, more accurately  $^{40}\text{Ca}$  core with eight  $f_{7/2}$  frozen neutrons. The single-particle energies for  $0f_{7/2}$ ,  $1p_{3/2}$ ,  $0f_{5/2}$ ,  $1p_{1/2}$ ,  $0g_{9/2}$  orbitals are 0.0, 2.0, 6.5, 4.0 and 9.0 MeV respectively. The relative single-particle energies are taken from the excitation energies of the low-lying negative parity states in  $^{49}\text{Ca}$ .<sup>2</sup>

### 2.2. Effective Interaction

For the  $fp$  valence space, an effective interaction with  $^{40}\text{Ca}$  as core has been reported in Ref.<sup>2</sup> This interaction has been built using  $fp$  two-body matrix elements (TBME) from Ref.<sup>28</sup> and  $1p_{3/2}$ ,  $0f_{5/2}$ ,  $1p_{1/2}$ ,  $0g_{9/2}$  TBME from Ref.<sup>24</sup> For the common active orbitals in these subspaces, matrix elements were taken from.<sup>24</sup> As the latter interaction has been defined for a  $^{56}\text{Ni}$  core, a scaling factor of  $A^{-1/3}$  amplitude is applied to take into account the change of radius between the  $^{40}\text{Ca}$  and  $^{56}\text{Ni}$  cores. As more and more neutrons are added in the  $f_{7/2}$  shell, the excitation energy of the  $9/2^+$  state decreases as reflected in Fig. 2 for  $^{41-71}\text{Sc}$  isotopes. The remaining matrix elements are taken from  $f_{7/2}g_{9/2}$  TBME from Ref.<sup>29</sup>

### 2.3. Monopole correction to the single-particle levels

As more and more neutrons are added in  $g_{9/2}$  orbital,  $f_{7/2}$  orbital becomes more repulsive and  $f_{5/2}$  more attractive. Thus proton  $f_{5/2}$  is pulled down while  $f_{7/2}$  is lifted up, as  $N$  increases, this is due to monopole interaction produced by tensor force between a proton in  $j_{>, <} = l \pm 1/2$  and a neutron in  $j'_{>, <} = l' \pm 1/2$ . Effects on  $p_{3/2}$  and  $p_{1/2}$  orbitals are small and can be neglected. In the present work, we have modified  $g_{9/2}f_{7/2}$  matrix elements by subtracting 100 keV and  $g_{9/2}f_{5/2}$  matrix elements by adding 100 keV. We have also check other set of values like 50 and 150 keV to modify  $g_{9/2}f_{7/2}$  and  $g_{9/2}f_{5/2}$  set of matrix elements. The results with 100

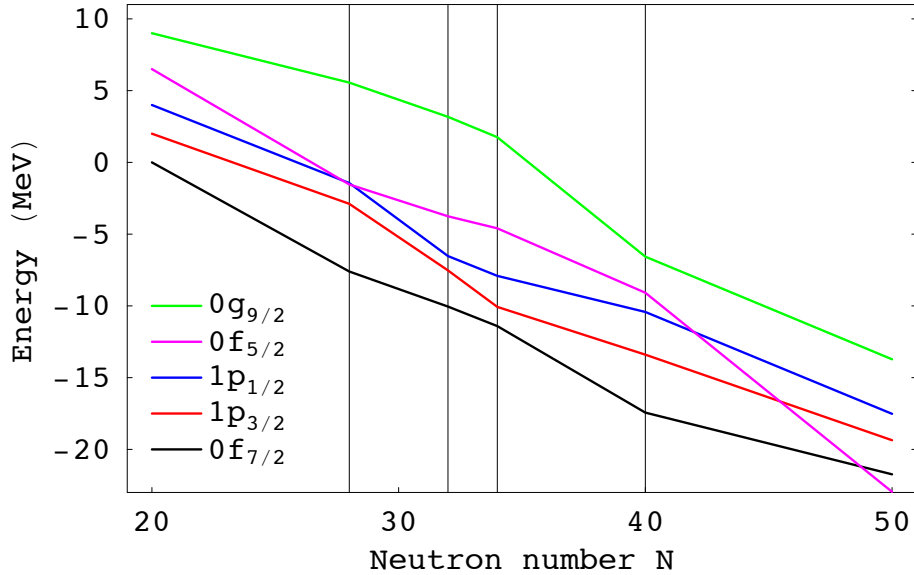
4 *P.C. Srivastava*

Fig. 2. Effective single-particle energies in  $^{41-71}\text{Sc}$  isotopes using  $pf_{g9}$  interaction.

keV modification is more reasonable. This modified interaction is named as  $pf_{g9a}$ . The effective single-particle energies for  $^{41-71}\text{Sc}$  isotopes are shown in Fig.3.

#### 2.4. State-of-the-art in the calculations

The modified interaction has been modified to reproduce the experimental data of Cu isotopes. These being odd nuclei, the available experimental data is sparse. The aim of this tuning is to first reproduce the ground state properties of  $^{75-79}\text{Cu}$  and then apply it to Ni and Zn isotopes. In the original  $fp_{g9}$  interaction,  $f_{5/2}$  level crosses the  $f_{7/2}$  at  $^{70}\text{Sc}$  and become lower in energy. This appears to be unrealistic.

In this modified interaction the  $f_{7/2}$  effective single-particle energy is always lower than  $f_{5/2}$  which is expected. Since the dimension of matrices involved for  $pf_{g9/2}$  space is very large, truncation of the full shell-model space are necessary. We have allowed neutron:  $t_{\nu}$  jumps from  $(p_{3/2}, f_{5/2}, p_{1/2})$  to  $g_{9/2}$ , protons:  $t_{\pi}$  jumps from  $f_{7/2}$  to  $(p_{3/2}, f_{5/2}, p_{1/2})$  orbital for each nucleus and each isotopes, an example of this truncation are shown in Fig. 4. We performed calculations for maximum dimension which are feasible by SGI-Cluster computer at GANIL. Up to this dimension, the states seems to be more convergent, which can be taken as the final result.

All the SM calculations have been carried out using the code ANTOINE <sup>24,30,31</sup> at SGI-Cluster computer at GANIL and DGCTIC-UNAM computational facility KanBalam.

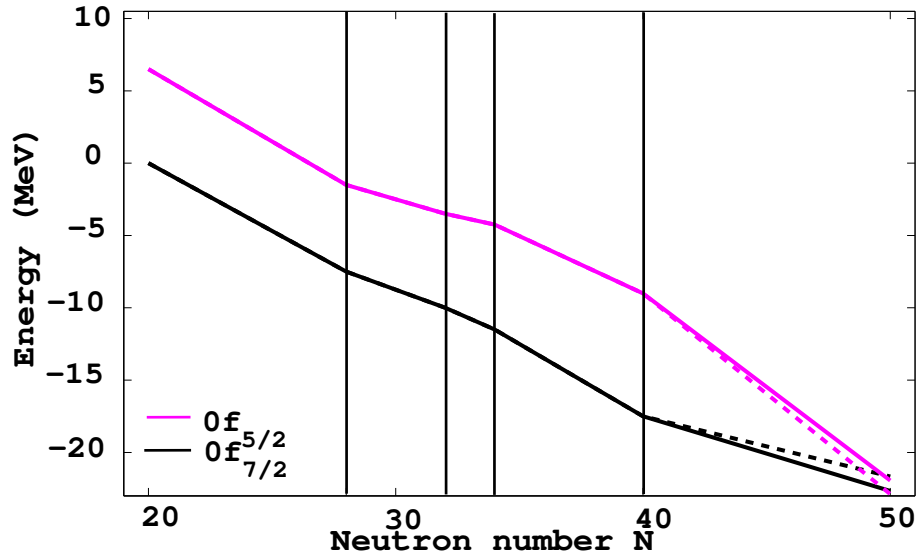


Fig. 3. Effective single-particle energies in  $^{41-71}\text{Sc}$  isotopes using  $pf9a$  interaction. In this figure, the results for  $pf9$  interaction are also shown as dotted lines.

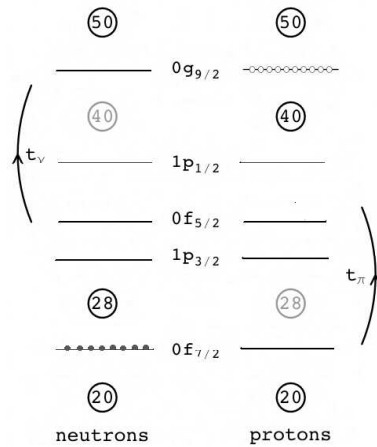


Fig. 4. Model space and truncation, neutron:  $t_\nu$  jumps from  $(p_{3/2}, f_{5/2}, p_{1/2})$  to  $g_{9/2}$ , protons:  $t_\pi$  jumps from  $f_{7/2}$  to  $(p_{3/2}, f_{5/2}, p_{1/2})$  orbital.

### 2.5. Binding Energies

To compare our shell model results with the experimental binding energies relative to binding energies of  $^{40}\text{Ca}$  we use following formula:

6 *P.C. Srivastava*

Table 1. The experimental (Expt.) and shell model (SM) g.s. energies. The values of energies are in MeV.

<sup>68</sup> Ni <sub>40</sub>		<sup>70</sup> Ni <sub>42</sub>		<sup>72</sup> Ni <sub>44</sub>		<sup>74</sup> Ni <sub>46</sub>		<sup>76</sup> Ni <sub>48</sub>			
Expt.	SM	Expt.	SM	Expt.	SM	Expt.	SM	Expt.	SM		
-248.3	-227.7	-260.2	-239.5	-271.1	-249.9	-281.7	-259.5	-293.7	-267.3		
<sup>69</sup> Cu <sub>40</sub>		<sup>71</sup> Cu <sub>42</sub>		<sup>73</sup> Cu <sub>44</sub>		<sup>75</sup> Cu <sub>46</sub>		<sup>77</sup> Cu <sub>48</sub>		<sup>79</sup> Cu <sub>50</sub>	
Expt.	SM	Expt.	SM	Expt.	SM	Expt.	SM	Expt.	SM	Expt.	SM
-257.9	-235.1	-271.0	-248.2	-283.4	-259.7	-294.7	-270.4	-305.4	-279.4	-315.2	-287.2
<sup>70</sup> Zn <sub>40</sub>		<sup>72</sup> Zn <sub>42</sub>		<sup>74</sup> Zn <sub>44</sub>		<sup>76</sup> Zn <sub>46</sub>		<sup>78</sup> Zn <sub>48</sub>		<sup>80</sup> Zn <sub>50</sub>	
Expt.	SM	Expt.	SM	Expt.	SM	Expt.	SM	Expt.	SM	Expt.	SM
-269.0	-242.6	-283.7	-257.4	-297.5	-271.8	-310.0	-283.6	-321.3	-293.5	-332.0	-302.4

$$E_B = -B_e = E(SM) + E_C + E_M. \quad (1)$$

In this Coulomb energies relative to <sup>40</sup>Ca given by <sup>32</sup>

$$E_C = e_\pi \pi + V_{\pi\pi} \frac{\pi(\pi-1)}{2} + V_{\pi\nu} \pi\nu + \left[\frac{1}{2}\pi\right] b_c, \quad (2)$$

where  $\pi(\nu)$  stands for the number of valence protons (neutrons) for <sup>40</sup>Ca core. We have taken the values of parameters  $e_\pi$ ,  $V_{\pi\pi}$ ,  $V_{\pi\nu}$  and  $b_c$  from Ref. <sup>32</sup> These parameters are determined by fitting to the measured Coulomb displacement energies of Ni( $Z=28$ ) $\leq Z \leq$  Mo( $Z=42$ ) with  $32 \leq N \leq 50$ . The resulting parameters are

$$e_\pi = 9.504 \text{ MeV}, V_{\pi\pi} = 0.228 \text{ MeV}, V_{\pi\nu} = -0.036 \text{ MeV}, b_c = 0.030 \text{ MeV}. \quad (3)$$

The monopole expression is given by <sup>33</sup>

$$E_M = e_\nu n + a \frac{1}{2} n(n-1) + b(T(T+1) - \frac{3}{4}n). \quad (4)$$

where  $n$  is total number of valence particles and  $T$  is the total isospin. The  $e_\nu$  is an average particle core interaction and  $a$  and  $b$  are the isoscalar and isovector global monopole correction. The values of the parameters at  $A = 42$  are <sup>33</sup>

$$e_\nu = -861 \pm 0.01 \text{ MeV}, a = 0.041 \pm 0.003 \text{ MeV}, b = 0.119 \pm 0.006 \text{ MeV}. \quad (5)$$

In Table 1, we have tabulated experimental (Expt.) and shell model (SM) g.s. energies.

### 3. Results and Discussion

The yrast levels for the nickel, copper and zinc isotopes for  $40 \leq N \leq 50$  are shown in Figs.5, 6 and 7.

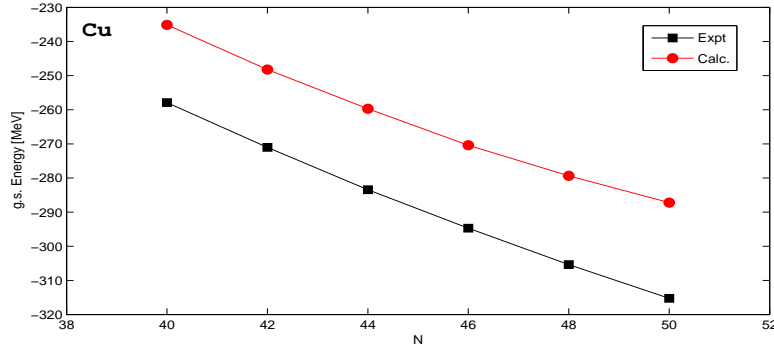


Fig. 5. Experimental <sup>34</sup> and calculated ground-state energies for Cu isotopes from A=69 to 79.

### 3.1. Copper isotopes

For <sup>69</sup>Cu, the ground state 3/2<sup>-</sup> is well predicted by *pfg9a* interaction. The calculated 1/2<sup>-</sup> and 5/2<sup>-</sup> state is reverse in comparison to experimental levels. The calculated 1/2<sup>-</sup> and 5/2<sup>-</sup> state is 134 keV and 378 keV lower in energy from the experimental levels. The order of 7/2<sub>1</sub><sup>-</sup>, 7/2<sub>2</sub><sup>-</sup> and 9/2<sup>-</sup> is well reproduced by this interaction. The 7/2<sub>2</sub><sup>-</sup> is only 62 keV below than experimental value. In <sup>69</sup>Cu, the 3/2<sup>-</sup> is interpreted by πp<sub>3/2</sub>, the 5/2<sup>-</sup> is interpreted by πp<sub>5/2</sub>. The first 7/2<sup>-</sup> is interpreted by πp<sub>3/2</sub>⊗2<sup>+</sup>(<sup>68</sup>Ni) and the second 7/2<sup>-</sup> is interpreted by πp<sub>7/2</sub><sup>-1</sup>.

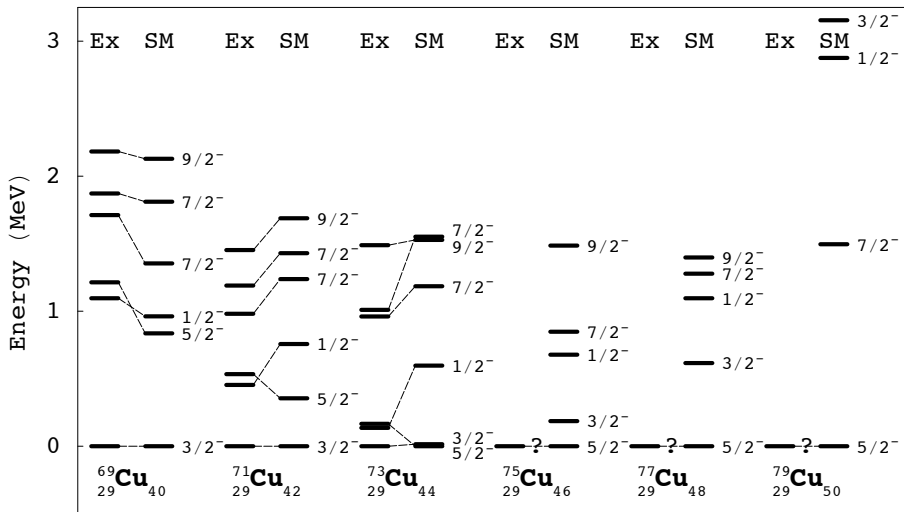


Fig. 6. Yrast levels of <sup>69–79</sup>Cu isotopes with *pfg9a* interaction.

The experimental and calculated ground-state energies for Cu isotopes are shown in Fig. 5. In Fig. 6, the yrast levels of  $^{69-79}\text{Cu}$  isotopes with  $pf g9a$  interaction are shown. For  $^{71}\text{Cu}$ , the ground state  $3/2^-$  is well predicted by  $pf g9a$  interaction. The order of  $5/2^-$  and  $1/2^-$  state is reverse in comparison to experimental levels. The calculated  $1/2^-$  level is 303 keV higher than the experimental value, while  $5/2^-$  level is 179 keV lower than the experimental result. The order of  $7/2_1^-$ ,  $7/2_2^-$  and  $9/2^-$  is well reproduced and are higher in energy from the experimental values. In the  $^{71}\text{Cu}$ , the  $3/2^-$  is interpreted by  $\pi p_{3/2}$ , and the  $5/2^-$  is interpreted by  $\pi p_{5/2}$ . The first  $7/2^-$  is interpreted by  $\pi p_{3/2} \otimes 2^+$  ( $^{70}\text{Ni}$ ) and the second  $7/2^-$  is interpreted by  $\pi p_{7/2}^{-1}$ .

For  $^{73}\text{Cu}$ ,  $pf g9a$  interaction predicts  $5/2^-$  state lower in energy by 15 keV from  $3/2^-$  state, while experimentally  $3/2^-$  is ground state.  $1/2^-$  state is 462 keV higher in energy from experimental value. The  $9/2^-$  lies in between two  $7/2^-$  states. In the  $^{73}\text{Cu}$ , the  $3/2^-$  is interpreted by  $\pi p_{3/2}$ , and the  $5/2^-$  is interpreted by  $\pi p_{5/2}$ . The first  $7/2^-$  is interpreted by  $\pi p_{3/2} \otimes 2^+$  ( $^{72}\text{Ni}$ ) and the second  $7/2^-$  is interpreted by  $\pi p_{7/2}^{-1}$ .

Recently, there is experimental indication of  $5/2^-$  as a ground state in  $^{75}\text{Cu}$  at REX-ISOLDE, CERN.<sup>10</sup> The  $pf g9a$  interaction also predicts  $5/2^-$  as a ground state. For  $^{77}\text{Cu}$  and  $^{79}\text{Cu}$ , this interaction predicts  $5/2^-$  as a ground state which is also expected from experiment. The calculations predict that the  $1/2^-$ ,  $9/2^-$  and  $7/2^-$  states are at very high in energy for  $^{79}\text{Cu}$  isotopes.

### 3.2. Nickel isotopes

The nickel isotopes ( $Z = 28$ ) cover three doubly-closed shells and therefore, a unique testing ground for large scale shell model calculations. Experimentally, the  $8^+$  isomerism though expected to be present in a whole chain from  $^{72}\text{Ni}$  to  $^{76}\text{Ni}$  was found to be suddenly absent in  $^{72}\text{Ni}$  and  $^{74}\text{Ni}$  and present in  $^{70}\text{Ni}$  and  $^{76}\text{Ni}$ . The ground state spin from  $^{68}\text{Ni}$  to  $^{76}\text{Ni}$  is correctly reproduced by  $pf g9a$  interaction.

The experimental and calculated ground-state energies for Ni isotopes are shown in Fig. 7. In Fig. 8, the yrast levels of  $^{68-76}\text{Ni}$  isotopes with  $pf g9a$  interaction are shown. For  $^{70}\text{Ni}$ , the first excited state  $2^+$  is calculated at 1.516 MeV which is 257 keV above than the experimental level. The states  $4^+$  at 2.229 MeV,  $6^+$  at 2.678 MeV, and  $8^+$  at 2.860 MeV are well predicted at 2.677 MeV, 2.958 MeV and 3.095 MeV. The agreement with the experimental data is reasonable. For  $^{72}\text{Ni}$  the first excited state  $2^+$  is calculated at 1.362 MeV which is 266 keV above the experimental level. The states  $4^+$  at 1.941 MeV and  $6^+$  at 2.396 MeV, are well predicted at 2.248 MeV and 2.470 MeV. Theoretically, there is  $8^+$  state at 2.621 MeV, but experimentally there is no indication of  $8^+$  isomeric states. For  $^{74}\text{Ni}$ , only two excited states are experimentally known. The first excited state  $2^+$  is calculated at 1.534 MeV which is 510 keV above the experimental value. The state  $4^+$  at 1.763



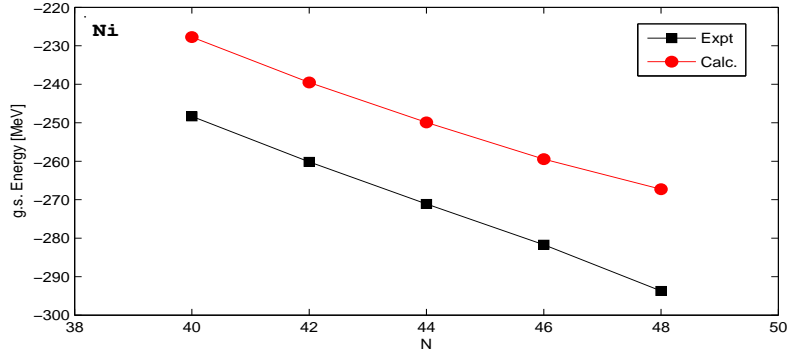


Fig. 7. Experimental  $^{34}$  and calculated ground-state energies for Ni isotopes from A=68 to 76.

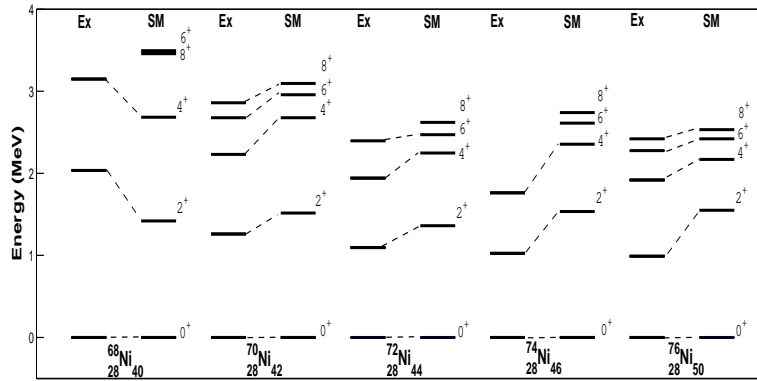


Fig. 8. Yrast levels of  $^{68-76}\text{Ni}$  isotopes with  $pf g9a$  interaction.

MeV is predicted at 2.354 MeV. The calculated  $6^+$ ,  $8^+$  state is at 2.612 MeV and 2.740 MeV respectively. For  $^{76}\text{Ni}$ , the calculated first  $2^+$  state is slightly higher in energy about 557 keV from the experimental value. The states  $4^+$  at 1.922 MeV,  $6^+$  at 2.276 MeV and isomeric states  $8^+$  at 2.420 MeV are well predicted at 2.169 MeV, 2.420 MeV and 2.532 MeV. The agreement for  $4^+$ ,  $6^+$  and  $8^+$  states with the experiment is good.

### 3.3. Zinc isotopes

The experimental and calculated ground-state energies for Ni isotopes are shown in Fig. 9. In Fig. 10, the yrast levels of  $^{70-80}\text{Zn}$  isotopes with  $pf g9a$  interaction are shown. The ground state spin for  $^{70-80}\text{Zn}$  isotopes for  $40 \leq N \leq 50$  is correctly

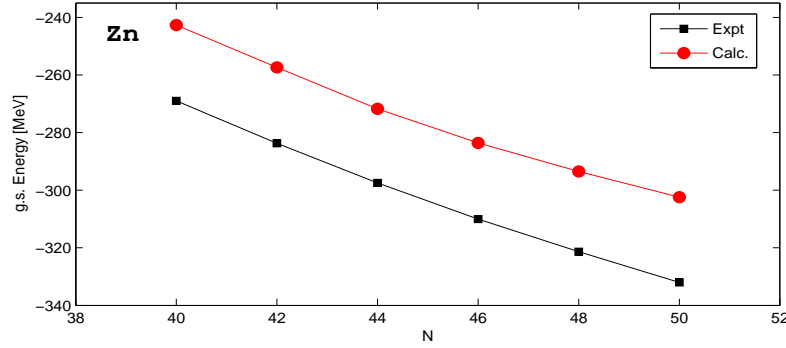


Fig. 9. Experimental  $^{34}$  and calculated ground-state energies for Zn isotopes from A=70 to 80.

reproduced by *pf<sub>g</sub>9a* interaction.

For  $^{70}\text{Zn}$ , the first excited  $2^+$  state is calculated at 0.603 MeV which is 282 keV below than experimental value. The states  $4^+$  at 1.79 MeV,  $6^+$  at 2.89 MeV and  $8^+$  at 3.75 MeV are well predicted at 1.47 MeV, 2.37 MeV and 2.53 MeV. The calculated values are compressed in comparison to the experimental value. For  $^{72}\text{Zn}$ , experimentally only  $2^+$  state at 0.653 MeV is known, which is predicted well by *pf<sub>g</sub>9a* interaction with energy difference of 74 keV. The calculated values of states  $4^+$ ,  $6^+$  and  $8^+$  are at 1.178, 1.923 and 2.601 MeV respectively. For  $^{74}\text{Zn}$ , the first excited  $2^+$  state is calculated at 0.825 MeV which is 219 keV above the experimental value. The state  $4^+$  at 1.419 MeV is predicted at 1.551 MeV. The states  $6^+$  and  $8^+$  are at 2.783 MeV and 3.430 MeV. For  $^{76}\text{Zn}$ , the first excited  $2^+$  state is calculated at 0.997 MeV which is 398 keV above the experimental value. The first  $4^+$  state is calculated with energy difference of 679 keV from the experimental value. The calculated  $4^+$ ,  $6^+$  and  $8^+$  states are at 1.975 MeV, 3.036 MeV and 3.243 MeV respectively. For  $^{78}\text{Zn}$ , the first excited  $2^+$  state is calculated at 1.307 MeV, which is 477 keV above the experimental value. The states  $4^+$  at 1.621 MeV,  $6^+$  at 2.528 MeV and  $8^+$  at 2.673 MeV are predicted at 2.247 MeV, 2.923 MeV and 2.955 MeV. Experimentally, the difference between  $6^+$  and  $8^+$  states is 145 keV while theoretically, it is only 32 keV. For  $^{78}\text{Zn}$ , the first excited  $2^+$  state is calculated at 1.953 MeV which is 461 keV smaller than the experimental value.

The calculated and experimental  $E(2_1^+)$  and  $E(4_1^+)$  for Ni and Zn isotopes are shown in Fig. 11. The high values of  $E(2_1^+)$  for Ni at N=40 is an indication of shell closure at N=40. For Zn isotopes, the  $E(2_1^+)$  and  $E(4_1^+)$  at N=40 and 50 are high in comparison to neighboring isotopes reflects shell closure at N=40 and N=50.

### 3.4. The $B(E2)$ systematics in the copper isotopes

The calculated values of first excited states of  $1/2^-$ ,  $5/2^-$  and  $7/2^-$  with its corresponding experimental values are shown in Fig. 12 for  $^{69-79}\text{Cu}$  isotopes. In the

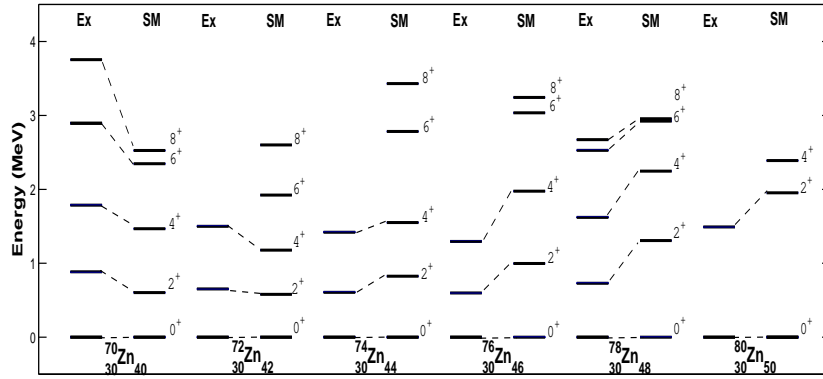


Fig. 10. Yrast levels of  $^{70-80}\text{Zn}$  isotopes with  $pf_{g9a}$  interaction.

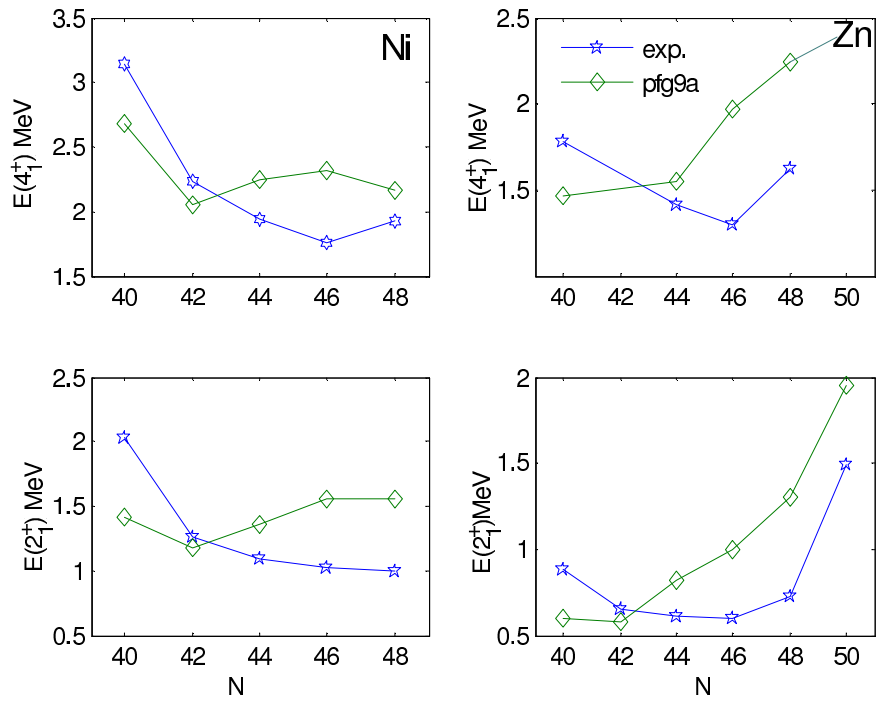


Fig. 11. The calculated and experimental  $E(2_1^+)$  and  $E(4_1^+)$  for Ni and Zn isotopes as a function of neutron number.

lower part of this figure, the calculated and experimental  $B(E2)$  values corresponding to different transitions namely,  $B(E2; 1/2^- \rightarrow 3/2^-)$ ,  $B(E2; 5/2^- \rightarrow 3/2^-)$  and

$B(E2; 7/2^- \rightarrow 3/2^-)$  are also shown. The calculated and experimental  $B(E2)$  values are tabulated in Table 2. The previously calculated value by Stefanescu *et al.* are shown within bracket.<sup>6</sup> The calculated  $B(E2; 1/2^- \rightarrow 3/2^-)$  values show much better agreement with experimental data compared to those of Stefanescu. The low  $B(E2)$  value beyond  $N=40$  for  $5/2^-$  state confirms its  $\pi f_{5/2}$  single-particle character. The sharp drop in the excitation energy of  $5/2^-$  state beyond  $N=40$  could be due to the monopole migration. The large  $B(E2)$  value for  $1/2^-$  state depart it from the single-particle character of  $\pi p_{1/2}$  type. The small  $B(E2; 7/2^- \rightarrow 3/2^-)$  values for  $^{73,75,77,79}\text{Cu}$  isotopes can be seen from wavefunctions of  $7/2^-$  and  $3/2^-$  states in Table 3, which show single-particle character of these states. In the first part of the Fig. 12, for the  $E(1/2^-)$  state the difference between predicted and experimental energy for  $^{69}\text{Cu}$ ,  $^{71}\text{Cu}$ ,  $^{73}\text{Cu}$  isotopes increases and its corresponding  $B(E2)$  value also increases.

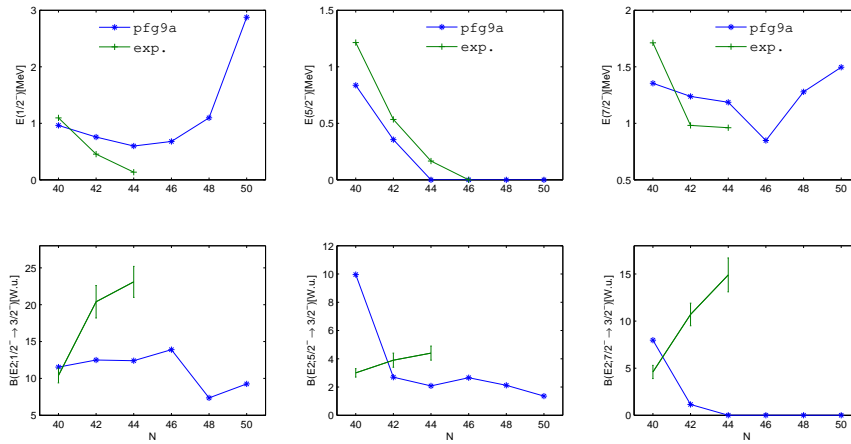


Fig. 12. The calculated and experimental  $B(E2)$  in W.u. for  $^{69-79}\text{Cu}$  isotopes. The shell model  $B(E2)$  values were calculated with the standard effective charges  $e_\pi = 1.5e$  and  $e_\nu = 0.5e$ .

### 3.5. The $B(E2)$ systematics in the nickel isotopes

The  $B(E2; 2_1^+ \rightarrow 0_1^+)$  value in  $^{68}\text{Ni}$  is much lower as compared to  $^{56}\text{Ni}$ . This low value was interpreted by Sorlin *et al.*<sup>2</sup> as originating from the enhanced neutron pair scattering at  $N = 40$ , which is referred to as superfluid behavior of the neutrons. The constancy of the  $B(E2)$  values beyond  $N = 40$  can be understood as follows:  $E2$  strength as  $np - nh$  excitation across  $N = 40$  for odd  $n$  cannot contribute due to parity conservation and for even  $n$  are dominated by pair scattering. Langanke *et al.*<sup>3</sup> performed microscopic calculations of the  $B(E2)$  in even-even nickel isotopes and

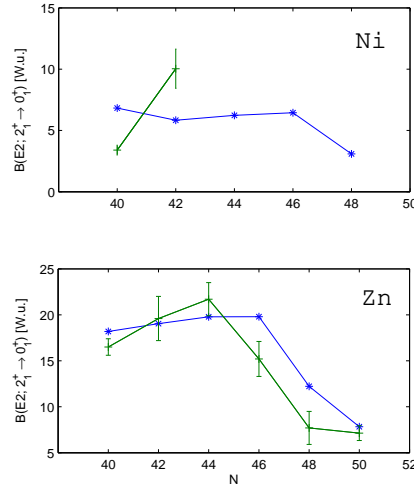


Fig. 13. The calculated and experimental  $B(E2; 2_1^+ \rightarrow 0_1^+)$  in W.u. for Ni and Zn isotopes as a function of neutron number. The shell model  $B(E2)$  values were calculated with the standard effective charges  $e_\pi = 1.5e$  and  $e_\nu = 0.5e$ .

found that the small observed  $B(E2)$  value is not necessarily an argument for a shell closure at  $N=40$ , but it simply reflects the fact that the lowest  $2^+$  state in  $^{68}\text{Ni}$  is primarily a neutron excitation. Van de Walle *et al.*<sup>35</sup> showed that  $B(E2)$  values in the Ni chain show a parabolic evolution between two magic numbers ( $N=28$  and  $40$ ), hinting a seniority-like behavior. Perru *et al.*<sup>4</sup> measured high  $B(E2)$  value for  $^{70}\text{Ni}$  at GANIL, and attributed it due to rapid proton core polarization when neutrons are added to the  $1g_{9/2}$  orbit. The calculated  $B(E2; 2_1^+ \rightarrow 0_1^+)$  values for  $^{68-76}\text{Ni}$  are shown in Fig. 13, the  $B(E2)$  value is almost constant from  $^{68-74}\text{Ni}$  and its value again decreases for  $^{76}\text{Ni}$ . This decrease in  $B(E2)$  value is probably due to oncoming of the next shell closure at  $N=50$  for  $^{78}\text{Ni}$ .

### 3.6. The $B(E2)$ systematics in the zinc isotopes

The experimental  $B(E2; 2_1^+ \rightarrow 0_1^+)$  values in the Zn isotopic chain show a similar trend towards  $N = 40$  as the Ni isotopes up to  $^{68}\text{Zn}$ . Though for  $^{70}\text{Zn}$  (at  $N = 40$ ), the  $B(E2)$  value suddenly increases. Leenhardt *et al.*<sup>36</sup> give three effects for supporting this increased collectivity: the addition of two protons out of the Ni core, the maximum in neutron pairing correlations at  $N = 40$ , and the presence of the strongly downslipping  $l = 4$  Nilsson neutron orbitals close to the Fermi surface. Kenn *et al.*<sup>37</sup> indicate that the inclusion of the  $1g_{9/2}$  orbit in the valence space is important in order to reproduce the increased  $B(E2; 2_1^+ \rightarrow 0_1^+)$  values in the  $^{70}\text{Zn}$ .

The calculated  $B(E2; 2_1^+ \rightarrow 0_1^+)$  values from present work using  $pf g9a$  interaction for  $^{70-80}\text{Zn}$  are shown in Fig. 13. The calculated value show similar trends as

14 *P.C. Srivastava*

experimental values from  $^{70}\text{Zn}$  to  $^{80}\text{Zn}$ . The  $B(E2)$  value at  $N=50$  is very low, this is an indication of shell closure at this value.

Table 2.  $B(E2)$  values (in W.u.) for  $^{69-79}\text{Cu}$  isotopes. The calculated results shown with corresponding value in the bracket from earlier work of Stefanescu *et al.*<sup>6</sup> The shell model  $B(E2)$  values were calculated with the standard effective charges  $e_\pi = 1.5e$  and  $e_\nu = 0.5e$ .

	$^{69}\text{Cu}_{40}$		$^{71}\text{Cu}_{42}$		$^{73}\text{Cu}_{44}$		$^{75}\text{Cu}_{46}$		$^{77}\text{Cu}_{48}$		$^{79}\text{Cu}_{50}$	
	Expt.	<i>pf g9a</i>	Expt.	<i>pf g9a</i>	Expt.	<i>pf g9a</i>	Expt.	<i>pf g9a</i>	Expt.	<i>pf g9a</i>	Expt.	<i>pf g9a</i>
$B(E2; 1/2^- \rightarrow 3/2^-)$	10.4[1.0]	11.5(7.1)	20.4[2.2]	12.5(7.3)	23.1[2.1]	12.41(7.5)	13.9	7.5	9.2			
$B(E2; 5/2^- \rightarrow 3/2^-)$	3.0[0.3]	9.9(1.6)	3.9[0.5]	2.7(1.7)	4.4[0.5]	2.07(1.3)	2.7	2.1	1.4			
$B(E2; 7/2^- \rightarrow 3/2^-)$	4.6[0.7]	7.9(1.2)	10.7[1.2]	1.2(1.5)	14.9[1.8]	0.0038(2.3)	0.0032	0.0002	0.0016			

Table 3. The calculated wave-function components of the lowest  $5/2^-$ ,  $3/2^-$ ,  $7/2^-$ , and  $1/2^-$  states in Cu isotopes.

	$5/2^-$		$3/2^-$		$7/2^-$		$1/2^-$	
$^{69}\text{Cu}_{40}$	12%	$\pi(f_{7/2}^8 p_{3/2}^1) \nu(f_{7/2}^8 p_{3/2}^4 f_{5/2}^4 p_{1/2}^2 g_{9/2}^2)$	31%	$\pi(f_{7/2}^8 p_{3/2}^1) \nu(f_{7/2}^8 p_{3/2}^4 f_{5/2}^4 p_{1/2}^2 g_{9/2}^2)$	22%	$\pi(f_{7/2}^8 f_{5/2}^1) \nu(f_{7/2}^8 p_{3/2}^4 f_{5/2}^4 p_{1/2}^2 g_{9/2}^2)$	16%	$\pi(f_{7/2}^8 p_{1/2}^1) \nu(f_{7/2}^8 p_{3/2}^4 f_{5/2}^4 p_{1/2}^2 g_{9/2}^2)$
$^{71}\text{Cu}_{42}$	18%	$\pi(f_{7/2}^8 f_{5/2}^1) \nu(f_{7/2}^8 p_{3/2}^4 f_{5/2}^4 p_{1/2}^2 g_{9/2}^4)$	24%	$\pi(f_{7/2}^8 p_{3/2}^1) \nu(f_{7/2}^8 p_{3/2}^4 f_{5/2}^4 p_{1/2}^2 g_{9/2}^4)$	14%	$\pi(f_{7/2}^8 f_{5/2}^1) \nu(f_{7/2}^8 p_{3/2}^4 f_{5/2}^4 p_{1/2}^2 g_{9/2}^4)$	13.5%	$\pi(f_{7/2}^8 p_{1/2}^1) \nu(f_{7/2}^8 p_{3/2}^4 f_{5/2}^4 p_{1/2}^2 g_{9/2}^4)$
$^{73}\text{Cu}_{44}$	17%	$\pi(f_{7/2}^8 f_{5/2}^1) \nu(f_{7/2}^8 p_{3/2}^4 f_{5/2}^6 p_{1/2}^2 g_{9/2}^4)$	34%	$\pi(f_{7/2}^8 p_{3/2}^1) \nu(f_{7/2}^8 p_{3/2}^4 f_{5/2}^6 p_{1/2}^2 g_{9/2}^4)$	15%	$\pi(f_{7/2}^8 f_{5/2}^1) \nu(f_{7/2}^8 p_{3/2}^4 f_{5/2}^6 p_{1/2}^2 g_{9/2}^4)$	11%	$\pi(f_{7/2}^8 p_{1/2}^1) \nu(f_{7/2}^8 p_{3/2}^4 f_{5/2}^6 p_{1/2}^2 g_{9/2}^4)$
$^{75}\text{Cu}_{46}$	35.5%	$\pi(f_{7/2}^8 f_{5/2}^1) \nu(f_{7/2}^8 p_{3/2}^4 f_{5/2}^6 p_{1/2}^2 g_{9/2}^6)$	36%	$\pi(f_{7/2}^8 p_{3/2}^1) \nu(f_{7/2}^8 p_{3/2}^4 f_{5/2}^6 p_{1/2}^2 g_{9/2}^6)$	11%	$\pi(f_{7/2}^8 f_{5/2}^1) \nu(f_{7/2}^8 p_{3/2}^4 f_{5/2}^6 p_{1/2}^2 g_{9/2}^6)$	19%	$\pi(f_{7/2}^8 f_{5/2}^1) \nu(f_{7/2}^8 p_{3/2}^4 f_{5/2}^6 p_{1/2}^2 g_{9/2}^6)$
$^{77}\text{Cu}_{48}$	60%	$\pi(f_{7/2}^8 f_{5/2}^1) \nu(f_{7/2}^8 p_{3/2}^4 f_{5/2}^6 p_{1/2}^2 g_{9/2}^8)$	47%	$\pi(f_{7/2}^8 p_{3/2}^1) \nu(f_{7/2}^8 p_{3/2}^4 f_{5/2}^6 p_{1/2}^2 g_{9/2}^8)$	41%	$\pi(f_{7/2}^8 f_{5/2}^1) \nu(f_{7/2}^8 p_{3/2}^4 f_{5/2}^6 p_{1/2}^2 g_{9/2}^8)$	50%	$\pi(f_{7/2}^8 f_{5/2}^1) \nu(f_{7/2}^8 p_{3/2}^4 f_{5/2}^6 p_{1/2}^2 g_{9/2}^8)$
$^{79}\text{Cu}_{50}$	79%	$\pi(f_{7/2}^8 f_{5/2}^1) \nu(f_{7/2}^8 p_{3/2}^4 f_{5/2}^6 p_{1/2}^2 g_{9/2}^{10})$	62%	$\pi(f_{7/2}^8 f_{5/2}^1) \nu(f_{7/2}^8 p_{3/2}^4 f_{5/2}^6 p_{1/2}^2 g_{9/2}^{10})$	74%	$\pi(f_{7/2}^8 f_{5/2}^1) \nu(f_{7/2}^8 p_{3/2}^4 f_{5/2}^6 p_{1/2}^2 g_{9/2}^{10})$	57%	$\pi(f_{7/2}^8 p_{1/2}^1) \nu(f_{7/2}^8 p_{3/2}^4 f_{5/2}^6 p_{1/2}^2 g_{9/2}^{10})$

#### 4. Conclusion

In the present work, the existing  $pf_{9/2}$  interaction for  $fp_{9/2}$  space with  $^{40}\text{Ca}$  core has been modified by changing  $\pi f_{5/2}\nu g_{9/2}$  and  $\pi f_{7/2}\nu g_{9/2}$  matrix elements. The new interaction is named as  $pf_{9/2}a$  has been tuned for Cu isotopes and tested for Ni and Zn isotopes. The  $pf_{9/2}a$  interaction give  $0^+$  ground state in an even-even nucleus like in Ni and Zn isotopes which is the characteristic of any reasonable interaction. These results indicate that further modification in interaction and even inclusion of  $1d_{5/2}$  orbit is important in the shell model calculations. The modification of Sorlin *et al.*, interaction is also attempted in,<sup>38</sup> but it will be remain to test this interaction is universal or not for this region. An attempt by including  $1d_{5/2}$  orbit in  $fp_{9/2}$  space to explain collectivity for  $fp$  shell nuclei is recently reported in.<sup>39</sup>

#### Acknowledgments

Thanks are due to Prof. P. Van Isacker and Prof. I. Mehrotra for suggestions during the work. All the calculations in the present paper are carried out using the SGI cluster resource at GANIL and DGCTIC-UNAM computational facility KanBalam. This work was supported in part by grants from the Sandwich PhD programme of the Embassy of France in India, Conacyt, México, and by DGAPA, UNAM project IN103212. I acknowledge fruitful discussions with Dr. M. J. Ermatov. The discussions with Prof. J. G. Hirsch and Prof. O. Civitarese is also acknowledge.

#### References

1. R. Broda *et al.*, Phys. Rev. Lett. **74**, 868 (1995).
2. O. Sorlin *et al.*, Phys. Rev. Lett. **88**, 092501 (2002).
3. K. Langanke *et al.*, Phys. Rev. C **67**, 044314 (2003).
4. O. Perru *et al.*, Phys. Rev. Lett. **96**, 232501 (2006).
5. H. Nakada *et al.*, Phys. Rev. C **81**, 051302 (2010).
6. I. Stefanescu *et al.*, Phys. Rev. Lett. **100**, 112502 (2008).
7. I. Stefanescu *et al.*, Phys. Rev. C **79**, 044325 (2009).
8. S.V. Ilyushkin *et al.*, Phys. Rev. C **80**, 054304 (2009).
9. J.M. Daugas *et al.*, Phys. Rev. C **81**, 034304 (2010).
10. K.T. Flanagan *et al.*, Phys. Rev. Lett. **103**, 142501 (2009).
11. K.T. Flanagan *et al.*, Phys. Rev. C **82**, 041302(R) (2010).
12. T. Otsuka *et al.*, Phys. Rev. Lett. **95**, 232502 (2005).
13. T. Otsuka *et al.*, Phys. Rev. Lett. **104**, 012501 (2010).
14. A. Gade *et al.*, Phys. Rev. C **81**, 051304(R) (2010).
15. W. Rother *et al.*, Phys. Rev. Lett. **106**, 022502 (2011).
16. P. C. Srivastava and I. Mehrotra, Int. J. Mod. Phys. E **20**, 637 (2011).
17. P. C. Srivastava and I. Mehrotra, J. Phys. G: Nuclear and Particle Physics **36**, 105106 (2009).
18. P. C. Srivastava and I. Mehrotra, Phys. At. Nucl. **73**, 1656 (2010).
19. P. C. Srivastava and I. Mehrotra, Eur. Phys. J. A **45**, 185 (2010).
20. P. C. Srivastava and V.K.B. Kota, Phys. At. Nucl. **74**, 971 (2011).
21. P. C. Srivastava, J. Phys. G: Nuclear and Particle Physics **39**, 015102 (2012).



22. P. C. Srivastava and I. Mehrotra, Int. J. Mod. Phys. E **21**, 1250007 (2012); arXiv:1112.4207 [nucl-th].
23. M.H. Jensen *et al.*, Phys. Rep. **261**, 125 (1995).
24. F. Nowacki, Ph.D. thesis (IRes, Strasbourg, 1996).
25. N. A. Smirnova, A. De Maesschalk, A. Van Dyck and K. Heyde, Phys. Rev. C **69**, 044306 (2004).
26. B.A. Brown and A.F. Lisetskiy (unpublished).
27. M. Honma, T. Otsuka, T. Mizusaki and M. Hjorth-Jensen, Phys. Rev. C **80**, 064323 (2009).
28. A. Poves, J. Sánchez-Solano, E. Caurier and F. Nowacki, Nucl. Phys. A **694**, 157 (2001).
29. S. Kahana, H. C. Lee, and C. K. Scott, Phys. Rev. **180**, 956 (1969).
30. E. Caurier, G. Martínez-Pinedo, F. Nowacki, A. Poves and A.P. Zuker Rev. Mod. Phys. **77**, 427 (2005).
31. E. Caurier, F. Nowacki, Acta Phys. Pol. B **30**, 705 (1999).
32. B.J. Cole, Phys. Rev. C **59**, 726 (1999).
33. E. Caurier, G. Martínez-Pinedo, F. Nowacki, A. Poves, J. Retamosa and A.P. Zuker, Phys. Rev. C **59**, 2033 (1999).
34. G. Audi, A.H. Wapstra and C. Thibault, Nucl. Phys. A **729**, 337 (2003).
35. J. Van de Walle *et al.*, Phys. Rev. Lett. **99**, 142501 (2007).
36. S. Leenhardt *et al.*, Eur. Phys. J. A **14**, 1 (2002).
37. O. Kenn *et al.*, Phys. Rev. C **65**, 034308 (2002).
38. K. Sieja and F. Nowacki, Phys. Rev. C **81**, 061303(R) (2010).
39. S.M. Lenzi, F. Nowacki, A.Poves and K. Sieja, Phys. Rev. C **82**, 054301 (2010).